INSTITUTE OF PHYSICS PUBLISHING and INTERNATIONAL ATOMIC ENERGY AGENCY NUCLEAR FUSION

Nucl. Fusion **43** (2003) 1653–1664 PII: S0029-5515(03)68967-2

The national spherical torus experiment (NSTX) research programme and progress towards high beta, long pulse operating scenarios

E.J. Synakowski[1], M.G. Bell[1], R.E. Bell[1], T. Bigelow[2], M. Bitter[1], W. Blanchard[1], J. Boedo[3], C. Bourdelle[4], C. Bush[2], D.S. Darrow[1], P.C. Efthimion[1], E.D. Fredrickson[1], D.A. Gates[1], M. Gilmore[5], L.R. Grisham[1], J.C. Hosea[1], D.W. Johnson[1], R. Kaita[1], S.M. Kaye[1], S. Kubota[6], H.W. Kugel[1], B.P. LeBlanc[1], K. Lee[7], R. Maingi[2], J. Manickam[1], R. Maqueda[8], E. Mazzucato[1], S.S. Medley[1], J. Menard[1], D. Mueller[1], B.A. Nelson[9], C. Neumeyer[1], M. Ono[1], F. Paoletti[10], H.K. Park[1], S.F. Paul[1], Y.-K.M. Peng[2], C.K. Phillips[1], S. Ramakrishnan[1], R. Raman[9], A.L. Roquemore[1], A. Rosenberg[1], P.M. Ryan[2], S.A. Sabbagh[10], C.H. Skinner[1], V. Soukhanovskii[1], T. Stevenson[1], D. Stutman[11], D.W. Swain[2], G. Taylor[1], A. Von Halle[1], J. Wilgen[2], M. Williams[1], J.R. Wilson[1], S.J. Zweben[1], R. Akers[12], R.E. Barry[2], P. Beiersdorfer[13], J.M. Bialek[10], B. Blagojevic[11], P.T. Bonoli[14], R. Budny[1], M.D. Carter[2], C.S. Chang[15], J. Chrzanowski[1], W. Davis[1], B. Deng[7], E.J. Doyle[16], L. Dudek[1], J. Egedal[14], R. Ellis[1], J.R. Ferron[16], M. Finkenthal[11], J. Foley[1], E. Fredd[1], A. Glasser[8], T. Gibney[1], R.J. Goldston[1], R. Harvey[17], R.E. Hatcher[1], R.J. Hawryluk[1], W. Heidbrink[18], K.W. Hill[1], W. Houlberg[2], T.R. Jarboe[9], S.C. Jardin[1], H. Ji[1], M. Kalish[1], J. Lawrance[19], L.L. Lao[16], K.C. Lee[7], F.M. Levinton[20], N.C. Luhmann[7], R. Majeski[1], R. Marsala[1], D. Mastravito[1], T.K. Mau[3], B. McCormack[1], M.M. Menon[2], O. Mitarai[21], M. Nagata[22], N. Nishino[23], M. Okabayashi[1], G. Oliaro[1], D. Pacella[24], R. Parsells[1], T. Peebles[6], B. Peneflor[16], D. Piglowski[16], R. Pinsker[16], G.D. Porter[12], A.K. Ram[14], M. Redi[1], M. Rensink[12], G. Rewoldt[1], J. Robinson[1], P. Roney[1], M. Schaffer[16], K. Shaing[25], S. Shiraiwa[26], P. Sichta[1], D. Stotler[1], B.C. Stratton[1], Y. Takase[26], X. Tang[8], R. Vero[11], W.R. Wampler[27], G.A. Wurden[8], X.Q. Xu[12], J.G. Yang[28], L. Zeng[6] and W. Zhu[6]

[1] Princeton Plasma Physics Laboratory, Princeton University, Princeton, NJ, USA
[2] Oak Ridge National Laboratory, Oak Ridge, TN, USA
[3] University of California, San Diego, CA, USA
[4] CEA Cadarache, France
[5] University of New Mexico at Albuquerque, Albuquerque, NM, USA
[6] University of California, Los Angeles, CA, USA
[7] University of California, Davis, CA, USA
[8] Los Alamos National Laboratory, Los Alamos, NM, USA
[9] University of Washington, Seattle, WA, USA
[10] Columbia University, New York, NY, USA
[11] Johns Hopkins University, Baltimore, MD, USA
[12] Euratom-UKAEA Fusion Association, Abingdon, Oxfordshire, UK
[13] Lawrence Livermore National Laboratory, Livermore, CA, USA
[14] Massachusetts Institute of Technology, Cambridge, MA, USA
[15] New York University, New York, NY, USA
[16] General Atomics, San Diego, CA, USA
[17] Compx, Del Mar, CA, USA
[18] University of California, Irvine, CA, USA
[19] Princeton Scientific Instruments, Princeton, NJ, USA
[20] Nova Photonics, Princeton, NJ, USA
[21] Kyushu Tokai University, Kumamoto, Japan
[22] Himeji Institute of Technology, Okayama, Japan
[23] Hiroshima University, Hiroshima, Japan
[24] ENEA, Frascati, Italy
[25] University of Wisconsin, Madison, WI, USA

0029-5515/03/121653+12$30.00

[26] Tokyo University, Tokyo, Japan
[27] Sandia National Laboratories, Albuquerque, NM, USA
[28] Korea Basic Science Institute, Taejon, Republic of Korea

E-mail: synakowski@pppl.gov

Received 12 November 2002, accepted for publication 25 August 2003
Published 1 December 2003
Online at stacks.iop.org/NF/43/1653

Abstract
A major research goal of the national spherical torus experiment is establishing long-pulse, high beta, high confinement operation and its physics basis. This research has been enabled by facility capabilities developed during 2001 and 2002, including neutral beam (up to 7 MW) and high harmonic fast wave (HHFW) heating (up to 6 MW), toroidal fields up to 6 kG, plasma currents up to 1.5 MA, flexible shape control, and wall preparation techniques. These capabilities have enabled the generation of plasmas with $\beta_T \equiv \langle p \rangle / (B_{T0}^2/2\mu_0)$ of up to 35%. Normalized beta values often exceed the no-wall limit, and studies suggest that passive wall mode stabilization enables this for H mode plasmas with broad pressure profiles. The viability of long, high bootstrap current fraction operations has been established for ELMing H mode plasmas with toroidal beta values in excess of 15% and sustained for several current relaxation times. Improvements in wall conditioning and fuelling are likely contributing to a reduction in H mode power thresholds. Electron thermal conduction is the dominant thermal loss channel in auxiliary heated plasmas examined thus far. HHFW effectively heats electrons, and its acceleration of fast beam ions has been observed. Evidence for HHFW current drive is obtained by comparision of the loop voltage evolution in plasmas with matched density and temperature profiles but varying phases of launched HHFW waves. Studies of emissions from electron Bernstein waves indicate a density scale length dependence of their transmission across the upper hybrid resonance near the plasma edge that is consistent with theoretical predictions. A peak heat flux to the divertor targets of 10 MW m^{-2} has been measured in the H mode, with large asymmetries being observed in the power deposition between the inner and outer strike points. Non-inductive plasma startup studies have focused on coaxial helicity injection. With this technique, toroidal currents up to 400 kA have been driven, and studies to assess flux closure and coupling to other current drive techniques have begun.

PACS numbers: 52.55.Fa, 52.25.Xz

1. Introduction

With the advent of significant levels of auxiliary heating and maturing diagnostic and operational capabilities in 2001 and 2002, the national spherical torus experiment (NSTX) [1] has begun intensive research aimed at establishing the physics basis for high performance, long pulse, solenoid-free operations of the spherical torus (ST) [2] concept. This research is directed at developing an understanding of the physics of the ST operational space, developing tools to expand this space, and contributing broadly to the science of toroidal confinement. To these ends, research has focused on high beta MHD stability, confinement, high harmonic fast wave (HHFW) heating and current drive, boundary physics, solenoid-free startup, and exploration of scenarios that integrate favourable confinement, stability, and non-inductive current drive properties. Some results of these efforts include the following:

- Toroidal beta values ($\beta_T \equiv \langle p \rangle / (B_{T0}^2/2\mu_0)$) of up to 35% have been obtained with neutral beam heating. In some plasmas at high normalized beta $\beta_N \equiv \beta_T/(I_p/aB_{T0})$, the no-wall stability limit is exceeded by 30%. Here, $\langle p \rangle$ is the volume-averaged pressure, B_{T0} is the vacuum field applied at the vessel centre, 'a' is the average minor radius of the plasma column, and I_p is the plasma current.
- Pulse lengths have been lengthened to 1 s with the benefit of bootstrap and beam-driven non-inductive currents of up to 60% of the total.
- Normalized beta values β_N up to 6.5% m T MA^{-1} have been achieved, with operations overall bounded by ratios of β_N to the internal inductance $l_i = 10$.
- Energy confinement times in plasmas with both L and H mode edges exceed the ITER98pby(2) scaling [3] by over 50%, and the ITER89-P L-mode scaling [4] by over a factor of two for both discharge types.
- Particle transport studies of plasmas with turbulent (L mode) edge conditions reveal impurity transport rates that are consistent with and in some cases fall below available neoclassical predictions in the core.
- Signatures of resistive wall modes have been observed [5, 6]. With sufficiently broad pressure profiles, their onset occurs above the calculated no-wall stability limit, pointing to the presence of passive wall stabilization.
- Tearing mode activity consistent with the expected behaviour of neoclassical tearing modes has been observed. These modes can saturate beta or cause beta reduction when the central value of the magnetic shear q is near unity, but for higher q values their effect on performance is modest.
- Several classes of fast-ion-induced MHD modes have been observed [7–9]. One of these, compressional Alfvén eigenmodes (CAEs), exists near the ion cyclotron frequency. The fact that CAE modes are a candidate for ion heating of the solar corona has motivated their study as a possible ion heating mechanism on NSTX. Also,

bounce-precession fishbone bursts are seen near 100 kHz, and are associated with fast ion losses.
- Significant heating of electrons with HHFWs has been measured [10]. Interactions between fast beam ions and HHFW have been observed.
- The first indications of current driven by HHFW have been obtained [10].
- The application of coaxial helicity injection (CHI) [11,12] has yielded a toroidal current of up to 400 kA, with observations of $n = 1$ MHD activity that may be a prerequisite for closed flux surface formation.
- Edge heat flux studies [13] using divertor infrared camera measurements indicate that 70% of the Ohmic and deposited neutral beam heating power flows to the divertor targets in quiescent H mode discharges.

In this paper, the operational capability and diagnostics are described in section 2. Section 3 summarizes three studies aimed at realizing high toroidal beta, demonstrating long pulse operations sustained by significant non-inductive current, and the combined realization of high beta and good confinement for durations longer than an energy confinement time. Section 4 contains summaries of topical research in MHD, confinement, HHFW, boundary physics, and CHI. Particular attention is given to those elements relevant to establishing the physics and operational basis for long pulse, high beta, high confinement regimes with high fractions of non-inductive current drive.

2. NSTX device description and facility capabilities

Some of the NSTX device characteristics [14] and facility capabilities are as follows. NSTX can generate plasmas with an aspect ratio R/a as low as 1.27. Plasma currents up to 1.5 MA have been obtained, and deuterium neutral beam injection (NBI) for heating and current drive is used routinely. Injected in the direction of the plasma current, the NBI system is capable of delivering 5 MW for up to 5 s. Powers up to 7 MW have been achieved for shorter periods of time. HHFW [15] can be delivered at variable phase for heating and current drive. Injected powers up to 6 MW have been achieved. NSTX has a close fitting conducting shell to maximize the plasma beta. The toroidal field capability ($B_{T0} \geqslant 0.6$ T) allows for pulse lengths up to 5 s at lower fields. Single- and double-null configurations can be generated, and elongations up to 2.5 and triangularities up to 0.8 have been achieved. Finally, the inner and outer halves of the vacuum vessel are electrically isolated from each other and can be biased for studies aimed at starting and sustaining the plasma non-inductively using CHI [11].

Operational improvements include the development of 350°C bakeout capability of the plasma-facing graphite tiles, implemented prior to the 2002 research campaign. This is part of a larger wall conditioning programme [16] that includes routine application of helium glow between shots to reduce impurity influxes, as well as boronization every few weeks of operation or as deemed necessary. Minimization of error fields by realignment of an outer poloidal field coil last year reduced the frequency of the onset of locked modes, widening the NSTX operating space. Finally, the capability of fuelling the plasma from the centre stack was implemented, motivated by work on the MAST device [17], complementing the outboard gas puffing capability. One result of these improvements was improved access to and reproducibility of H modes.

A schematic cross-section of NSTX is shown in figure 1 [18, 19]. Central to NSTX research is a suite of diagnostics [20], including a multi-timepoint Thomson scattering system (20 radial points for these studies, covering the high field side to low field side, at up to 60 Hz sampling) that is absolutely calibrated for both density and temperature profile measurements. Carbon ion temperature and toroidal rotation measurements are made using charge exchange recombination spectroscopy (CHERS). For the data described herein, the CHERS data were obtained with a time resolution of 20 ms and 17 radial channels spanning the outer half of the plasma cross-section. These measurements are facilitated by a dedicated background view that enables direct subtraction of background emission that lies in the spectral range of the desired charge-exchange-induced signal. Ultra-soft x-ray measurements made using three arrays, displaced toroidally and poloidally, enable core MHD instabilities to be identified. An array of magnetic sensors on the centre stack, as well as the outboard side of the plasma, permit magnetic equilibrium reconstruction and identification of toroidal number of external modes. A fast magnetic coil sensor system enables measurements of MHD perturbations at several times the ion cyclotron frequency (up to 10 MHz), in the range of CAEs [8]. A scanning neutral particle analyser measures the fast ion distribution function, including distortions induced by fast ion absorption of energy from the HHFWs. Infrared cameras have enabled the first studies of edge heat flux scalings.

The key to progress in research on NSTX has been the development of a flexible shaping and position control system. High triangularity and elongation raises the edge q for a fixed current and toroidal field. Owing to the strong in–out variation of the toroidal field, the shaping can be particularly beneficial to low aspect ratio devices such as NSTX, including the realization of higher values of I/aB_{T0} as compared to those achievable on larger aspect ratio devices. Strong early shaping enables the avoidance of early MHD, enabling rapid current ramps of up to 5 MA s^{-1} to be used at the start of an NSTX pulse. This combination of shaping and fast ramps also yields comparatively broadened current profiles that increase MHD stability limits and thus allow higher beta values to be achieved. Figure 2 shows the plasma equilibrium for the NSTX discharge with a toroidal beta of 35%. The equilibria are evaluated from magnetics-based equilibrium reconstructions using the EFIT code [21]. Recently, a control algorithm based on real-time EFIT (rtEFIT) [22] reconstructions, originally developed at DIII-D, has been implemented. This is aimed at yielding improved position, shape and feedback control in future experimental campaigns.

3. High beta, long pulse and high confinement plasmas

3.1. High beta operations

The low aspect ratio and strong shaping capability on NSTX has enabled the realization of high beta plasmas. Shown in figure 3 are time traces from the plasma with the highest β_T yet obtained. Run in the double-null configuration at 0.3 T,

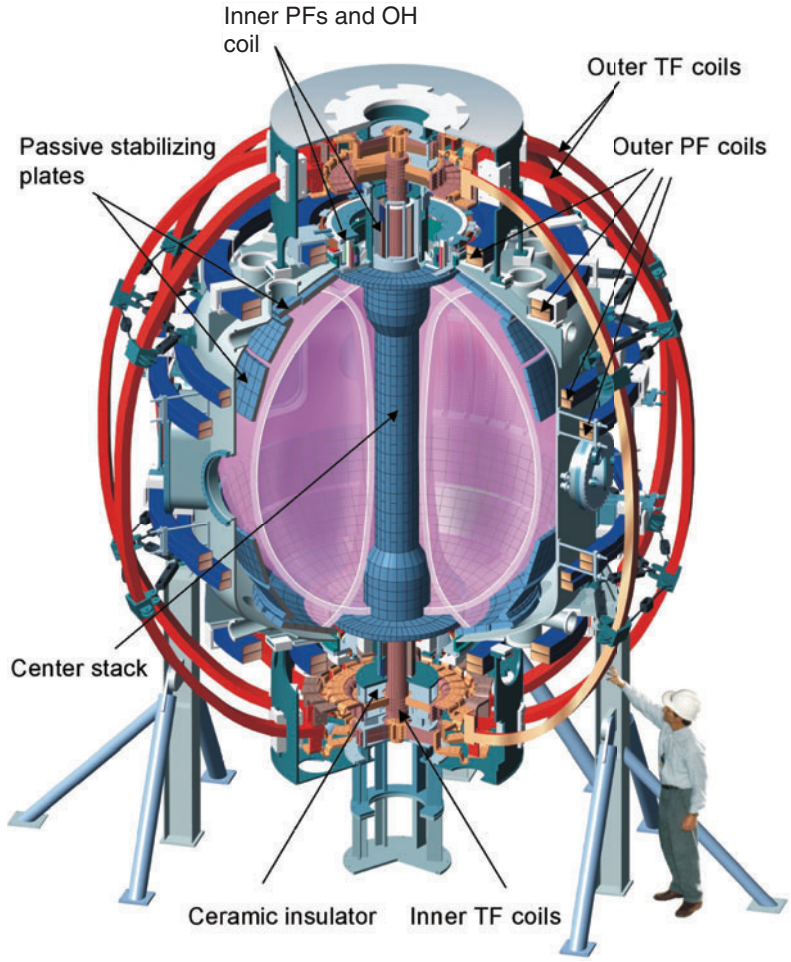

Figure 1. Schematic cut-out view of the NSTX device.

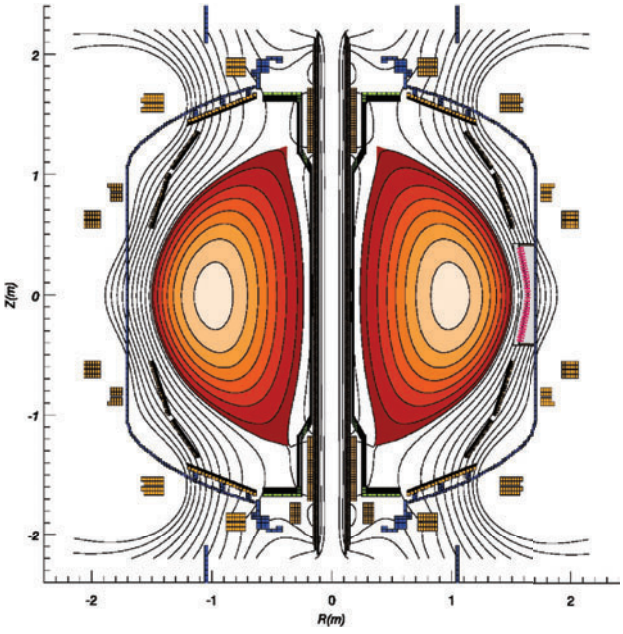

Figure 2. Surfaces of constant magnetic flux for a neutral-beam-heated plasma with a toroidal beta of 35% (shot 108989). The plasma had an applied toroidal field of 0.3 T, aspect ratio of 1.4, elongation of 2.0 and triangularity of 0.8.

this plasma reached β_T of 35%. The maximum β_N was 6.3, below the no-wall limit. This discharge entered a dithering H mode state near 230 ms, which transited to an ELM-free state after 260 ms. Beta saturation was associated with the onset of an internal 1/1 mode. Depletion of available volt–seconds led to the termination of this discharge.

3.2. Long pulses with significant non-inductive current

One important goal for ST research in the long term is the achievement of high fractions of current driven by non-inductive means. Progress towards this has been realized through the generation of plasmas with a non-inductive current fraction of up to 60%, sustained for a duration on the order of the current penetration time [23] (figure 4). In these 0.45 T, 800 kA plasmas, $\beta_T = 15$–20%. Stability analysis with the DCON [24] code indicates that this plasma, with β_N of about 6, was well above the no-wall stability limit, suggesting that passive wall stabilization played a role in its sustainment. Neutral beam current drive and bootstrap currents yielded low surface voltage of 0.1 V for a time period of the order of the estimated current relaxation time [25] of about 200 ms. Calculations based on the neoclassical formulation of [26] indicate that late in the low loop voltage phase, more than half of the non-inductive current comes from the bootstrap

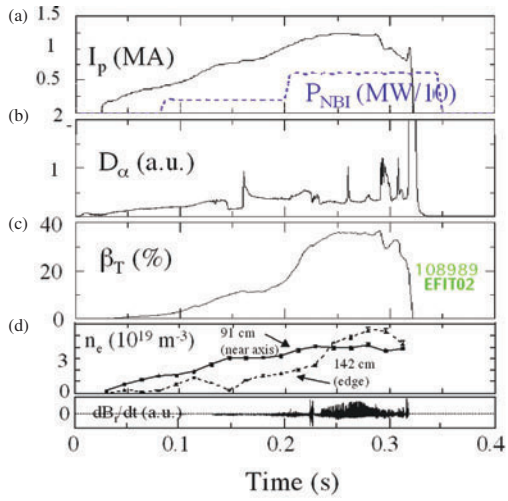

Figure 3. Characteristics of a neutral-beam-heated, double-null plasma that obtained a maximum volume-averaged beta of 35%. (*a*) Plasma current and NBI power. (*b*) D_α emission. (*c*) Volume-averaged toroidal beta β_T. (*d*) Electron density, measured with absolutely calibrated Thomson scattering, at a location near the magnetic axis and near the plasma periphery on the midplane. (*e*) MHD activity as measured by a Mirnov coil for a double-null plasma. The plasma had an applied toroidal field of 0.3 T, aspect ratio of 1.4, elongation of 2.0, triangularity of 0.8, internal inductance of 0.6, and a central q as determined from magnetics analysis of 1.4. During the high beta period, the plasma enters an H mode, as evidenced by the drop in D_α and broadening of the density profile.

effect. The total pulse lengths for these neutral-beam-heated H mode plasmas extends to 1 s, with 700 ms current flattops. Early neutral beam heating and the rapid current ramp combined to reduce the plasma's internal inductance by yielding comparatively high edge current densities and slow current diffusion rates in the early phase of the discharge. Also, the development of an increased edge bootstrap current is calculated to be associated with the H mode edge pedestal.

The pulse length was not limited by flux consumption. Rather, MHD activity at 650 ms that appears to be related to the q profile and pressure profile evolution initiated the first drop in the core beta. The details of this MHD are still under investigation. Measurements of core MHD activity with soft x-ray arrays are consistent with the hypothesis that a double tearing mode that follows the generation of magnetic shear reversal is responsible for the degradation. Confirming this awaits a direct measurement of the magnetic shear. As for increasing the performance and pulse length of these plasmas, success in combining effective HHFW with neutral beam heating could have a significant impact on the plasma resistivity and bootstrap current. Modification of the q profile evolution with HHFW in this manner, and ultimately with HHFW aimed at direct current drive, represents a major research thrust for NSTX in the upcoming research campaign.

3.3. Simultaneous achievement of high stored energy and high confinement

Higher toroidal field operations led to the highest stored energies yet achieved in NSTX (figure 5), and the highest combined products of beta and confinement enhancement

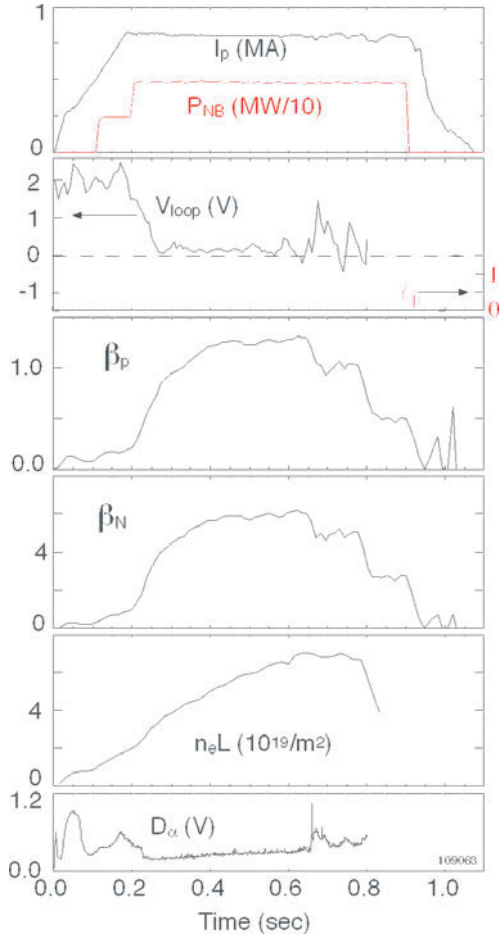

Figure 4. The plasma current, injected beam power, surface voltage, internal inductance, beta poloidal, normalized beta, line density and D_α emission for an NSTX discharge with over 50% non-inductive current drive. The plasma transited to H mode shortly after the addition of the second neutral beam source.

factor. These plasmas had an applied toroidal field of 0.55 T, higher than that used in the highest beta plasmas and near the operational limit of 0.6 T. For this plasma, $\beta_N H_{89L}$, where H_{89L} is the ratio of the measured confinement time to that predicted by the ITER L mode scaling relation, is 12 or higher for eight energy confinement times, illustrating that high performance can be maintained on NSTX for durations sufficient for the study of the physics of high beta, high confinement regimes.

4. Topical research

4.1. MHD

4.1.1. Beta limiting modes. The simultaneous realization of high values of normalized beta and low internal inductance is one component of demonstrating the attractiveness and viability of wall-stabilized, high bootstrap fraction operations of the ST [27]. Research on NSTX in 2001 and 2002 has extended the range of β_T, β_N, β_N/l_i, and pulse length achieved in a toroidal confinement device of this scale. These plasma states have been achieved with confinement times that meet or exceed expectations based on scaling laws developed from moderate aspect ratio tokamak experiments in both the L and H mode regimes (as described in section 4.2).

Some aspects of the operating space realized thus far on NSTX are illustrated in figure 6. At present, this operating space lies below $\beta_N/l_i = 10$. One targeted operating point for NSTX plasmas is characterized by β_N of 8 at l_i of 0.2–0.3 and is based on an assumption of broad pressure profiles so as to maximize the bootstrap current and stability. Achieving the highest values of β_N simultaneously with the lowest values of internal inductance demands that NSTX operate beyond the no-wall stability limit. Stability calculations [6] indicate that it is only for $\beta_N > 5$ that global MHD modes exhibit magnetic perturbations with poloidal wavelengths sufficiently long for effective wall coupling. Since at lower values of β_N many combinations of pressure peaking, internal inductance and shape yield configurations that are ideally unstable, a research challenge is finding a self-consistent path to these high β_N configurations. To date, the path that has most successfully led to this corner of the NSTX operating space has utilized rapid current ramps, early neutral beam heating, shaping and transitions to the H mode that yield broad pressure profiles and low values of the pressure peaking factor, F_p. H mode pressure profiles also have benefits with respect to ideal stability, bootstrap current generation and large plasma volume with high energy content. It should be pointed out, however, that plasmas with L mode edges in NSTX also exhibit high confinement and toroidal beta values that approach or even exceed 30% (see section 4.2.1).

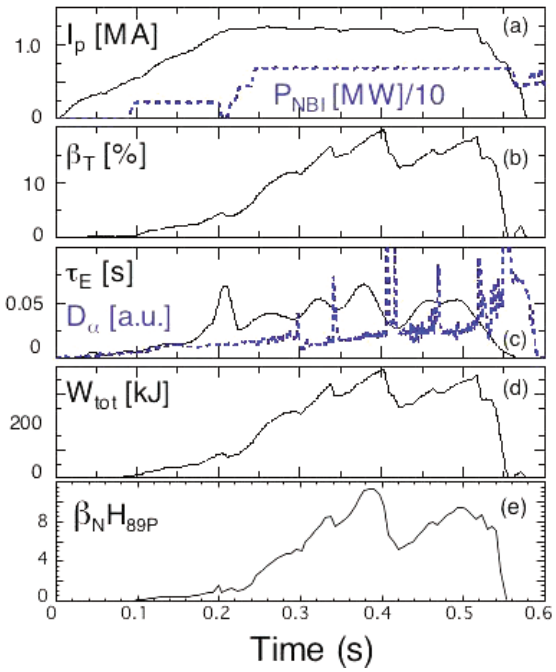

Figure 5. Data for a plasma that obtained 390 kJ of stored energy. An H mode transition occurred at 300 ms. (*a*) Plasma current and neutral beam heating power. (*b*) Toroidal beta. (*c*) Energy confinement time and D_α emission. (*d*) Stored energy, determined from analysis of magnetics data. (*e*) The product of the normalized beta with the confinement enhancement factor H_{89P}.

Analysis of many plasmas with high β_N indicates that the no-wall stability limit has been exceeded, and that wall stabilization is likely a critical player in achieving this state. Shown in figure 7 are β_N and the central rotation for a discharge that exceeds the no-wall stability limit as calculated by the DCON code. The no-wall limit for the $n = 1$ mode is surpassed for about 3.5 wall times. Significantly, the collapse of high plasma stored energy and falling below the no-wall limit is preceded by a reduction of the plasma rotation, suggesting that the wall mode stabilization that is enabled by this rotation is lost at some critical rotation frequency. A detailed analysis of passive wall stabilization in high β_N NSTX plasmas is provided in [6].

Tearing mode activity, probably neoclassical tearing modes, has been observed on NSTX to saturate beta in some cases, as well as to degrade overall performance. These modes are slowly growing and, in many shots, are identified as 1/1, 2/1 and 3/2 islands. The mode growth is consistent with that predicted by the modified Rutherford equation [28]. These modes are most easily avoided by operating plasmas with elevated $q(0)$, which is consistent with the desired final high performance state of low internal inductance operation.

A recent theoretical study [29] reveals that the theoretical ideal beta limits of moderate aspect ratio tokamaks and STs can be viewed in a unified fashion if the standard definition

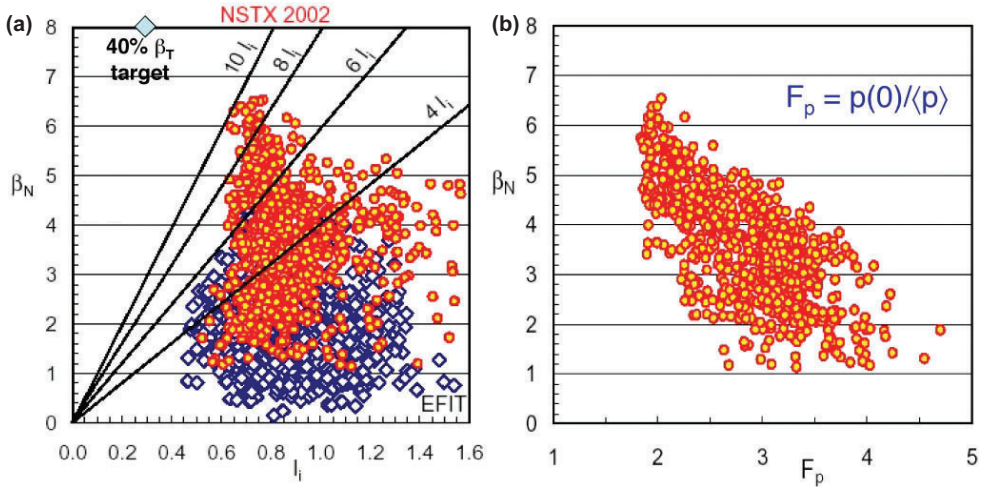

Figure 6. The achieved values of (*a*) β_N versus plasma internal inductance, and (*b*) β_N versus pressure peaking factor for NSTX in the 1999 through 2002 research campaigns. The lighter points are data obtained in the 2002 campaign. Beta and internal inductance are determined with EFIT code analysis of magnetics data.

of beta is broadened. It is found that the normalized beta limits over a wide range of aspect ratio are similar if the volume-averaged magnetic field pressure $\langle\beta\rangle \equiv 2\mu_0\langle p\rangle/\langle B^2\rangle$ is used to define $\langle\beta_N\rangle \equiv \langle\beta\rangle(\%)aB_{T0}/I_p(\mathrm{MA})$, where B_{T0} is the applied vacuum magnetic field at the plasma major radius. Figure 8 shows a database of normalized beta values using both the usual definition and this modified definition. The band outlined in figure 8 shows the stability limit for moderate and small aspect ratio achieved in the theoretical study, along with the NSTX data. These plasmas exceed this theoretical limit, suggesting that some stabilization mechanism is at work.

4.1.2. Fast beam-ion-induced MHD modes. In general, STs are susceptible to fast ion driven instabilities due to the relatively low toroidal field. Indeed, a wide variety of such instabilities has been seen in NSTX at frequencies ranging from a few kilohertz to many megahertz [9]. In the frequency range below about 200 kHz, a form of the fishbone or energetic particle mode has been seen, as well as modes that appear to be similar to the TAE modes of conventional tokamaks (figure 9). Unlike in conventional tokamaks, the frequency ranges of these two classes of instabilities have substantial overlap, complicating the experimental identification and theoretical analysis. Significant fast ion losses have been correlated, under some conditions, with the appearance of both of these types of modes.

In the higher frequency ranges, up to 5 MHz and perhaps higher, observed modes may be related to the various forms of ion cyclotron emission (ICE) of conventional tokamaks. This theory has recently been extended to the ST geometry and indicates that much of the near-ion-cyclotron-frequency MHD observed on NSTX may consist of global Alfvén eigenmodes (GAE) and CAEs destabilized by the fast ion population [30]. Their presence could impact fast ion distributions and thus, ultimately, fast ion confinement, but no clear experimental evidence exists for this as yet.

An experiment has been performed in conjunction with the DIII-D tokamak that takes advantage of the similar cross-sectional shapes and area, but different aspect ratios. Toroidal Alfvén eigenmodes (TAE) modes were identified at similar frequencies in both but at higher mode numbers on DIII-D, as expected by theory. Also, the threshold in beam beta for beam-driven instabilities is similar in both devices.

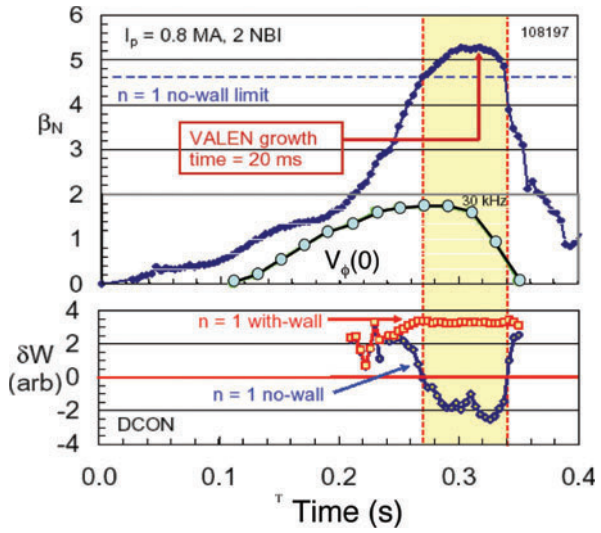

Figure 7. β_N and central carbon rotation velocity as a function of time. This plasma exceeds the no-wall stability limit, as identified by the DCON code, for several wall times. The loss of stability is preceded by a reduction of the plasma rotation. The potential energy δW for $n = 1$ modes is positive if the effects of the nearby conducting walls are included in the stability analysis, indicating that these modes should be stable under these conditions. By assuming that the conducting walls are absent, these modes are predicted to be unstable.

4.2. *Confinement and transport*

4.2.1. Global confinement. The confinement times in neutral-beam-heated NSTX plasmas compare favourably to the ITER-89P empirical scaling expression [4] as well as the ITER98pby(2) scaling rule (figure 10) [31, 32]. This is true for plasmas with distinct H mode transitions as well as for L mode edge plasmas. An interesting aspect of this relation between the H and L mode states can be seen in figure 3. At the H mode transition (near 230 ms), a change in plasma beta and stored energy is not noticeable. While an increase in the rate of change of stored energy is usually observed in L to H transitions, these other cases are prompting analysis of the local changes of transport properties in the core and edge across an L to H mode transition.

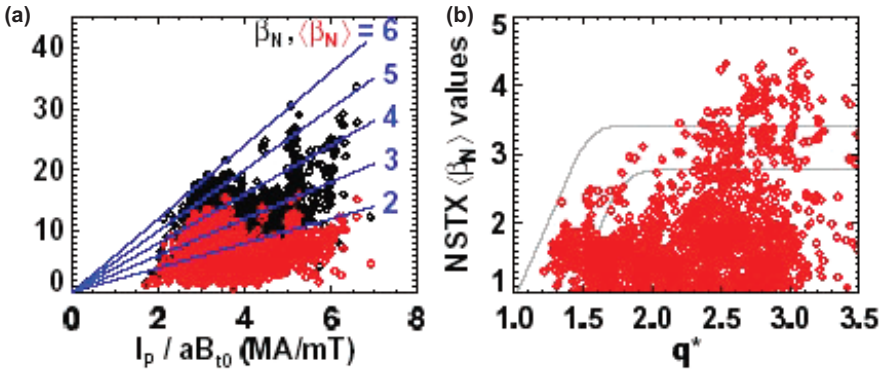

Figure 8. (*a*) β_T (black) and $\langle\beta\rangle$ (red) at maximum stored energy for NBI-heated plasmas plotted against normalized current. Constant β_N lines are shown. (*b*) $\langle\beta_N\rangle$ versus $q*$ for the discharges from (*a*) (from [29]).

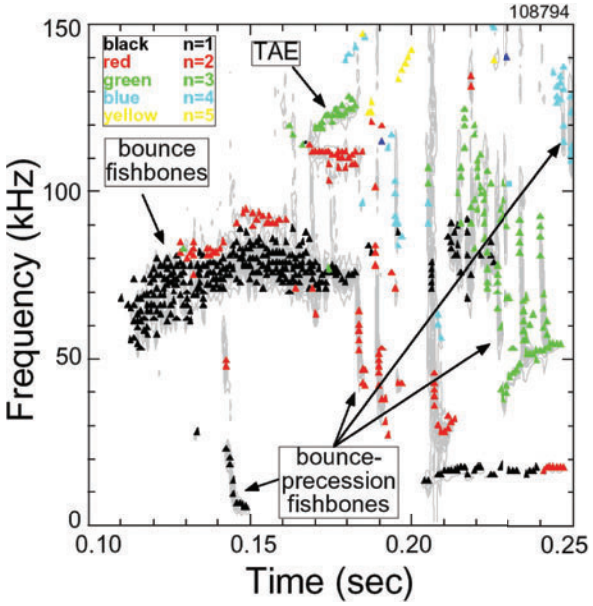

Figure 9. A sampling of the energetic particle modes often observed on NSTX neutral-beam-heated discharge.

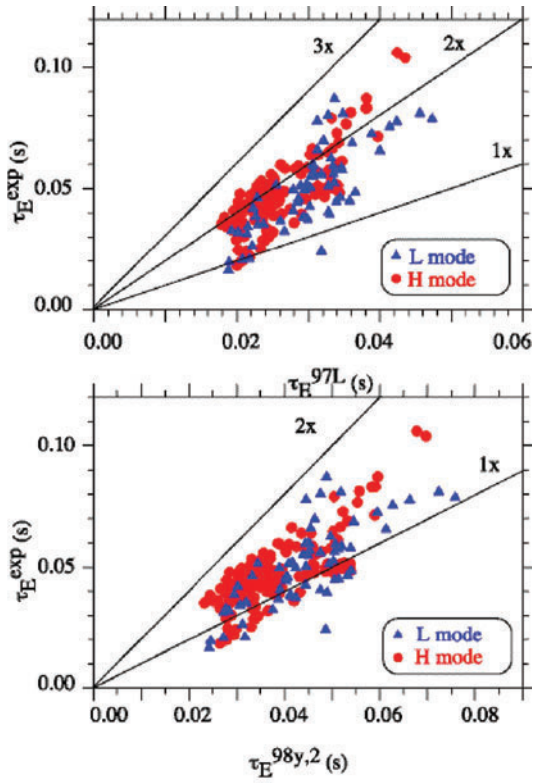

Figure 10. Energy confinement times, determined with magnetics analysis, compared to values calculated from the two ITER scaling expressions. Data for plasmas with both L and H mode edges are shown.

4.2.2. H mode access, dynamics and power balance. H mode operations have become routine on NSTX, aided by improved wall conditioning and reduced error fields. Access to the H mode is easiest in the lower single-null (LSN) configuration, but H modes have been obtained in double-null as well. This is

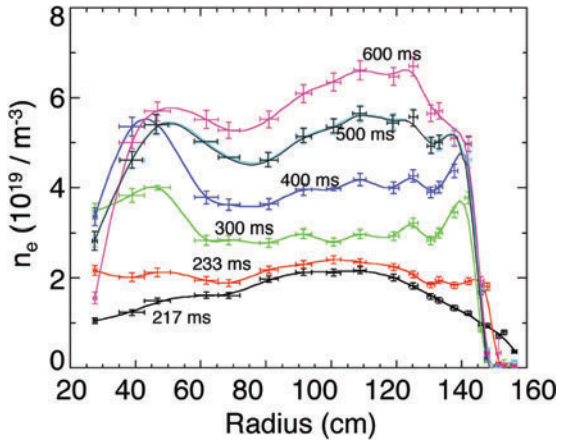

Figure 11. Density evolution in the long-pulse H mode described in figure 4.

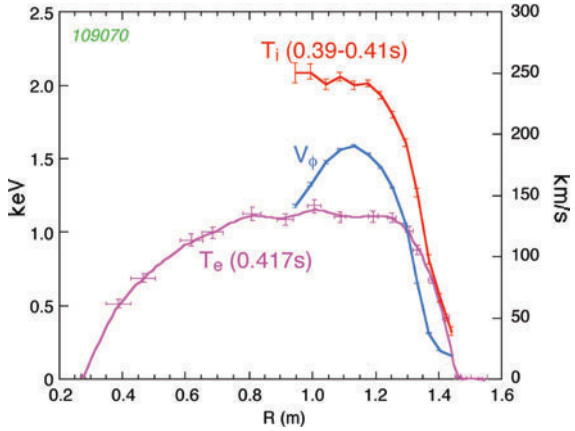

Figure 12. T_i, T_e and toroidal rotation V_ϕ in the long pulse H mode discharge described in figure 4.

to be contrasted with observations made on the MAST device, where double-null plasmas exhibit the lowest power thresholds [33]. A power threshold of several hundred kilowatts is observed in some cases and exhibits a secular fall as the NSTX wall conditions improve [34].

The evolution of the density of the long-pulse H mode plasma described in section 3.2 can be seen in figure 11. Of note is the presence of pronounced 'ears' in the electron density profile that arise shortly after the L to H transition, likely a signature of an edge particle transport barrier. Similar density profile characteristics have been observed on MAST [35] and START [36].

A time slice of the profile measurements of the electron temperature T_e, the ion temperature T_i and the rotation velocity V_ϕ are shown in figure 12. The high T_i compared to T_e is a persistent feature seen in most NSTX neutral-beam-heated discharges. Along with expectations that neutral beam fast ion energy should be transferred predominantly to the electrons in this temperature range, this suggests that the dominant loss channel is electron thermal conduction. Power balance analyses yield ion thermal conductivities χ_i that are of the order of predictions from neoclassical theory and electron thermal conductivity χ_e that is significantly larger than χ_i. The momentum diffusivity χ_ϕ is smaller than χ_i in this analysis, qualitatively consistent with expectations

from neoclassical theory. It should be noted that analysis of some discharges under the usual assumptions of classical ion–electron energy exchange and neoclassical fast ion slowing down and transport leads to the conclusion that ion heat fluxes can fall below neoclassical levels and can even be opposite the usual direction in some cases. The surprising character of these results is prompting reassessments of this analysis on many fronts, including recalibration of diagnostic systems, investigation of ion heating from stochastic MHD modes driven by super-Alfvénic beam ions [9], and the possible damping of electron temperature gradient (ETG) modes on thermal ions. Low transport in the ion channel is also found with impurity ions. Analysis of neon gas puffing suggests that the impurity diffusion is near neoclassical levels in the core of L mode plasmas. Microinstability analysis of beam-heated plasmas using the GS2 gyrokinetic code [37] is being performed to assess the roles of long wavelength ion temperature gradient (ITG) and trapped electron modes (TEMs), as well as shorter wavelength ETG modes. Further details of NSTX core confinement studies can be found in [38]

4.2.3. Edge turbulence measurements. Three different measurement techniques have been implemented to measure turbulence characteristics in the plasma scrape-off layer. All of them—an edge reciprocating Langmuir probe, edge reflectometry and gas puff imaging [39]—reveal highly turbulent SOL activity in the L mode. The edge probe and imaging point to the presence of intermittent convective transport events. These results will be compared to developing theory of these nonlinear transport phenomena. Studies will focus on assessing their role in determining the overall radial heat transport to the divertor.

4.3. RF heating and current drive

4.3.1. High harmonic fast wave. A campaign to explore the physics and the application of HHFW heating has been carried out on the NSTX device with the ultimate goal of providing a tool for long pulse, high beta ST operation. RF wave energy is launched into the NSTX plasma at a frequency of 30 MHz via a 12-element antenna array. The elements can be phased to launch a variety of wave spectra with toroidal wave numbers between $\pm 14\,\mathrm{m}^{-1}$.

As expected from theory [15], electron heating has been observed for a wide variety of plasma conditions and over the full range of applied wave spectra. Electron temperatures as high as 3.7 keV have been produced (figure 13). Heating efficiency, characterized by the value of the central electron temperature, seems to be highest for the slowest wave phase velocities. NSTX plasmas with predominantly electron heating exhibit a strong degradation in confinement, which is consistent with theoretical predictions of an increase in conduction due to ETG modes [40]. Attempts to measure the power deposition profile with modulated rf power have also showed a very stiff temperature profile response consistent with a marginally stable profile. Some discharges are characterized by an apparent barrier in the T_e profile, and by reduced electron conduction in the central region. Long duration (400 ms) steady rf driven H modes at moderate plasma current $I_p = 350$ kA with β_p near unity, and bootstrap current fraction of 40% have been created. These H modes have continuous ELM activity and are not accompanied by a strong increase in density or Z_{eff}. H modes at higher values of plasma current have been ELM-free, with steadily increasing density until the termination after only a brief 40 ms interval.

Experiments with directed wave spectra have been conducted to investigate the possibility of driving plasma current. Differences between co- and counter-directed HHFW waves have been observed in the loop voltage (figure 14) and in the MHD behaviour, which are consistent with current being driven on axis in the expected direction. Careful matching of the electron temperature and density are required to make meaningful comparisons between the shots. For the best-matched cases at $\pm 7\,\mathrm{m}^{-1}$ a driven current of about 100 kA is inferred from the loop voltage, in reasonable agreement with predictions from the TORIC full wave code [41] and a factor of two smaller than that estimated from the CURRAY ray tracing code [42]. Loop voltage differences have also been observed for faster wave phase velocities down to $\pm 2.4\,\mathrm{m}^{-1}$. An interesting and not understood effect is that differences in central heating efficiency are also found between co- and counter-phasing with counter-phasing being up to twice as

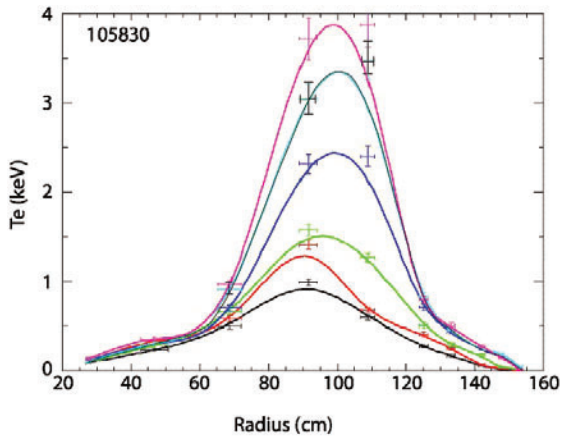

Figure 13. Electron temperature for a plasma heated with 3.5 MW HHFW. Data acquisition times were separated by 16.7 ms.

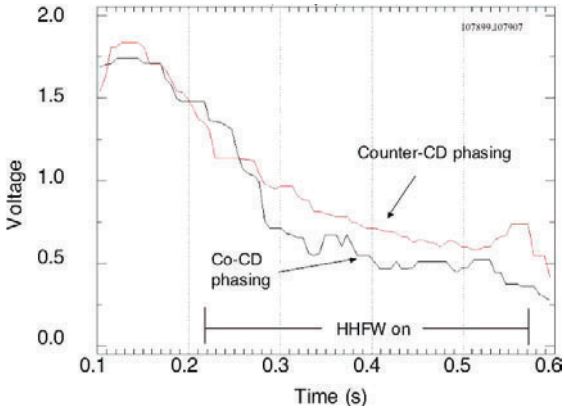

Figure 14. Surface loop voltage for two HHFW-heated plasmas with co- and counter-antenna phasing. The n_e and T_e profiles were matched by adjusting the heating power to be 2.2 MW co-phasing, 1.2 MW counter-phasing.

efficient. Theory predicts no substantial difference in heating efficiency for the opposed spectra.

Ion heating provides a potential alternate channel for rf absorption that can lower the efficiency of the current drive. Despite the large values of cyclotron harmonic involved (9–14), significant wave damping is expected at large values of the ion beta. Acceleration of neutral-beam-injected 80 keV ions to 140 keV has been observed. The ion tail is strongest at the highest values of toroidal field. The flux of particles accelerated by the HHFW. The flux also shows a small dependence on wave spectrum. The flux decreases with increasing phase velocity, in contrast to theoretical predictions of the opposite behaviour. No dependence on plasma current was observed and the observed dependence on injection energy shows a weaker interaction at lower voltage.

4.3.2. Electron Bernstein wave emission studies. In NSTX and other ST plasmas, the electron plasma frequency far exceeds the electron cyclotron frequency and, as a consequence, conventional ECE $T_e(R)$ diagnostics, electron cyclotron heating, and electron cyclotron current drive techniques cannot be used. In contrast, electron Bernstein waves (EBWs) readily propagate in ST plasmas and absorb strongly at ECE resonances, making them potentially attractive as a $T_e(R)$ diagnostic or for heating and current drive. However, in order to propagate beyond the upper hybrid resonance (UHR) that surrounds the ST plasma, the EBWs must mode convert to electromagnetic waves. In magnetic fusion research, this mode conversion process was first studied on the W7-AS stellarator [43]. On NSTX, EBW emission, mode-converted to extraordinary electromagnetic (X-mode) waves, has been measured with an 8–18 GHz swept-frequency radiometer [10]. These EBW emission studies are essential not only for the development of a $T_e(R)$ diagnostic, but also for understanding the mode conversion physics that is an important prerequisite for developing viable EBW heating and current drive scenarios. The mode conversion of EBWs to X-mode is sensitively dependent on the density scale length (L_n) at the UHR, which for fundamental EBWs is normally located in the scrape-off region of an ST.

On NSTX, a sudden, threefold increase in EBW conversion efficiency has been observed during H mode transitions (figure 15). Similar results were obtained on the MAST device [44]. This increase is due to the natural steepening of the edge density profile at the L to H transition. The measured EBW to X mode conversion efficiency during the H mode on NSTX is consistent with the theoretical mode conversion efficiency derived using measured L_n data. A fourfold increase in the EBW mode conversion efficiency was measured when the density scale length (L_n) was progressively shortened by a local boron nitride limiter in the scrape-off of an ohmically heated L mode plasma. The maximum conversion efficiency approached 50% when L_n was reduced to 0.7 cm, in agreement with theoretical predictions and consistent with results obtained on the CDX-U device [45]. Calculations indicate that it will be possible to establish $L_n < 0.3$ cm with a local limiter, a value predicted to be necessary to attain the required >80% EBW conversion to the X mode for proposed EBW heating and current drive scenarios on NSTX.

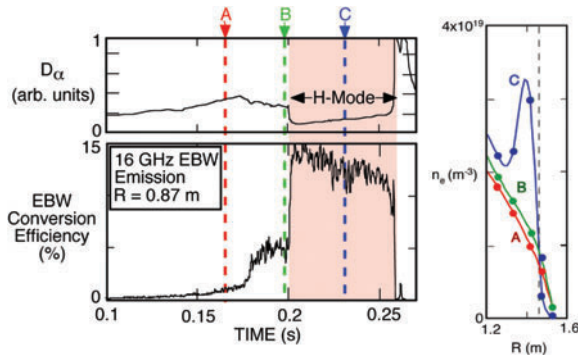

Figure 15. EBW emission measured for a plasma that transits to H mode near 0.2 s. Three edge density profiles for the times marked by the dashed lines and measured by Thomson scattering are shown on the right.

4.4. Boundary physics

Boundary physics research in NSTX focuses on power and particle balance. High heat flux on the target plate has been measured in LSN divertor plasmas. For example, the peak heat flux in a LSN ELM-free H mode plasma with 4.5 MW of heating power has reached 10 MW m^{-2}, with a full-width half-maximum of 2 cm at the outer target plate [34], approaching the spatial resolution of the infrared camera used to make the measurement (figure 16). Peak heat flux in H mode plasmas increases with NBI heating power. The peak heat flux at the inboard target is typically 0.5–1.5 MW m^{-2}, with a profile full-width half-maximum of ~10 cm. The power flowing to the inboard side is typically 0.2–0.33 of the outboard power (figure 15). The outer target tile heating and incident power appear to be higher in L mode plasmas than in ELM-free H mode plasmas, whereas the heating of inboard sides is comparable.

A tile temperature increase of 300°C has been measured during the first 0.2 s after divertor establishment in H modes. Extrapolation of the temperature rise, assuming an increase ~(time)$^{1/2}$ with constant peak heat flux, yields a tile temperature in excess of the 1200°C engineering limit after ~3 s. While this limitation should not impact the NSTX near-term programme of investigating pulse lengths up to several energy confinement times, more detailed study is required to assess the power handling requirements for pulse lengths in excess of several current penetration times (beyond 1 s) at the highest available input powers. As pulse lengths are increased in NSTX, the emphasis in boundary physics research

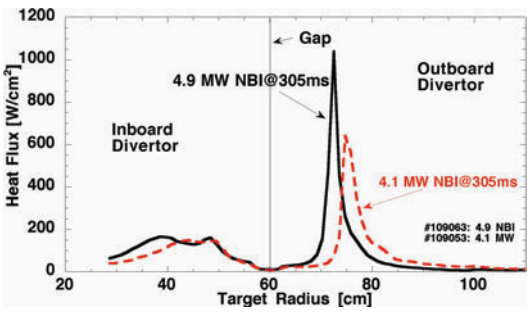

Figure 16. Divertor heat flux in two quiescent H modes, one with 4.1 MW injected NB power, the other with 4.9 MW.

will be placed on using double-nulls, radiative divertor/mantle solutions, and X-point sweeping.

4.5. Coaxial helicity injection

Strategies for initiating current non-inductively on NSTX by the process of CHI [11, 12] are being developed. CHI is implemented on NSTX by driving current along field lines that connect the inner and outer lower divertor plates. A description of the CHI system on NSTX can be found in [46]. A 50 kA, 1 kV DC power supply is connected across the inner and outer vessel components, which are insulated from each other by ceramic rings at the bottom and top. The CHI method drives current initially on open field lines, creating a current density profile that is hollow and intrinsically unstable. Taylor relaxation predicts a flattening of this current profile through a process of magnetic reconnection leading to current being driven throughout the volume, with some being carried on closed flux surfaces.

The applied injector voltage determines the amount of injector current that can be driven for each combination of toroidal field, injector flux and gas pressure. This flux is defined as the difference in poloidal flux between the upper and lower insulating gaps separating the inner and outer electrodes. In the discharge shown in figure 17, as the injector voltage is increased and the injector flux reduced, the toroidal current reaches nearly 400 kA. The injector current is 28 kA, which results in a current multiplication factor of 14, roughly equal to the theoretical maximum attainable. During the high current phase after 200 ms, there are oscillations in the toroidal current signal. It is not known if these are signatures of reconnection events that lead to closed flux plasma that then decays, only to be re-established. In high current discharges such as this, a magnetic perturbation with amplitude 2 mT measured at the outboard midplane and toroidal mode number $n = 1$ is observed, rotating toroidally in the $E_r \times B_p$ direction with a frequency in the range 5–12 kHz. Such a mode, which has been seen on high current CHI discharges on HIT and HIT-II, may be a signature of the formation of closed flux surfaces.

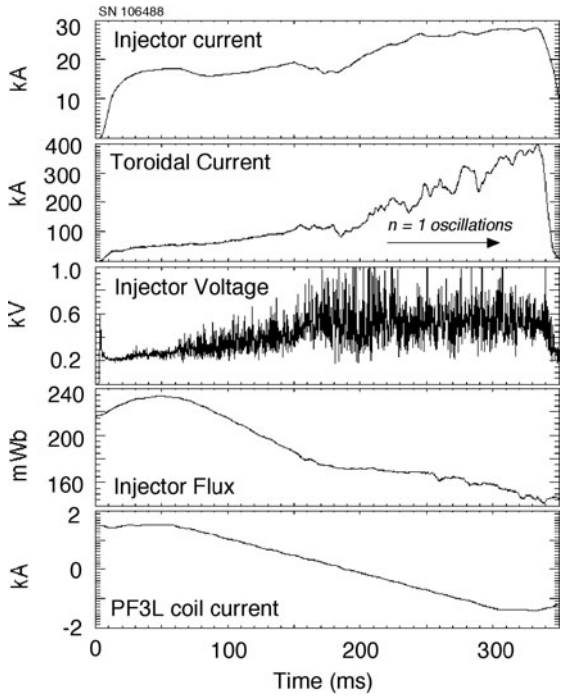

Figure 17. Injector parameters, toroidal current and coil current in a CHI discharge.

To improve the reliability and performance of the CHI system, the absorber region has been modified to suppress arcs, and feedback control should help to retain the closed flux that may be created in future higher current CHI discharges, a necessary step in performing a successful handoff to other current drive scenarios. A new short pulse discharge initiation method, developed on HIT-II, will be investigated on NSTX for the purposes of handing off a CHI discharge to a inductively driven plasma [47].

Acknowledgment

This research was supported by DoE contract DE-AC02-76CH03073.

References

[1] Ono M. *et al* 2000 *Proc. 18th Int. Conf. on Fusion Energy 2000 (Sorrento, 2000)* (Vienna: IAEA) CD-ROM file EX7/5 and http://www.iaea.org/programmes/ripc/physics/fec2000/html/node1.htm
[2] Peng Y.-K.M. and Strickler D.J. 1986 *Nucl. Fusion* **26** 769
[3] The ITER Team 1999 *Nucl. Fusion* **39** 2137
[4] Yushmanov P.N. *et al* 1990 *Nucl. Fusion* **30** 1999
[5] Sabbagh S.A. *et al* 2001 *Nucl. Fusion* **41** 1601
[6] Sabbagh S.A. *et al* 2002 *Proc. 19th Int. Conf. on Fusion Energy 2002 (Lyon, 2002)* (Vienna: IAEA) CD-ROM file EX/S2-2 and http://www.iaea.org/programmes/ripc/physics/fec2002html/fec2002.htm
[7] Gorelenkov N.N. and Cheng C.Z. 1995 *Nucl. Fusion* **35** 1743
[8] Fredrickson E.D. *et al* 2001 *Phys. Rev. Lett.* **87** 145001
[9] Gates D., White R. and Gorelenkov N. 2001 *Phys. Rev. Lett.* **87** 205003
[10] Ryan P.M. *et al* 2002 *Proc. 19th Int. Conf. on Fusion Energy 2002 (Lyon, 2002)* (Vienna: IAEA) CD-ROM file EX/P2-13 and http://www.iaea.org/programmes/ripc/physics/fec2002html/ fec2002.htm
[11] Jarboe T.R. *et al* 1998 *Phys. Plasmas* **5** 1807–14
[12] Jarboe T.R. *et al* 1998 *Proc. 17th Int. Conf. on Fusion Energy 1998 (Yokohama, 1998)* (Vienna: IAEA) CD-ROM file PDP/2 and http://www.iaea.org/programmes/ricp/physics/start.htm
[13] Maingi R. *et al* 2002 Recent results from the national spherical torus experiment *Proc. 11th Int. Conf. on Plasma Physics (Sidney, Australia, 2002) (Plasma Phys. Control. Fusion* at press)
[14] Ono M. *et al* 1999 *Proc. 18th IEEE/NPSS Symp. on Fusion Engineering (Albuquerque, NM 1999)* (Piscataway, NJ: IEEE) p 53
[15] Ono M. 1995 *Phys. Plasmas* **2** 4075
[16] Kugel H.W. *et al* 2001 *J. Nucl. Mater.* **290–293** 1185
[17] Sykes A. *et al* 1995 *Proc. 15th Int. Conf. on Plasma Physics and Controlled Nuclear Fusion Research 1994 (Seville, 1994)* vol 1 (Vienna: IAEA) p 719
[18] Neumeyer C. *et al* 1999 National spherical torus experiment (NSTX) construction, commissioning, and initial operations *Proc. 18th IEEE/NPSS Symp. on Fusion Engineering (Albuquerque, NM 1999)* (Piscataway, NJ: IEEE)
[19] Chrzankowski J. *et al* 1999 National spherical torus experiment (NSTX) torus design, fabrication, and assembly *Proc. 18th IEEE/NPSS Symp. on Fusion Engineering (Albuquerque, NM 1999)* (Piscataway, NJ: IEEE)

[20] Kaita R. *et al* 2001 NSTX diagnostics for fusion plasma science studies *Proc. 28th Int. Conf. on Plasma Science (ICOPS)/13th Int. Pulsed Power Plasma Science (PPPS-2001) (Las Vegas, NV, 17–22 June 2001)*
[21] Lao L.L. *et al* 1990 *Nucl. Fusion* **30** 1035
[22] Ferron J.R. *et al* 1998 *Nucl. Fusion* **38** 1055
[23] Menard J.E. *et al* 2003 *Nucl. Fusion* **43** 330
[24] Glasser A.H. and Chance M.S. 1997 *Bull. Am. Phys. Soc.* **42** 1848
[25] Mikkelesun D.R. 1989 *Phys. Fluids* B **1** 333
[26] Sauter O. *et al* 2000 *Phys. Plasmas* **7** 1224
[27] Menard J.E., Jardin S.C. and Kaye S.M. *et al* 1997 *Nucl. Fusion* **37** 595
[28] Sauter O. *et al* 1997 *Phys. Plasmas* **4** 1654
[29] Menard J. *et al Phys. Plasmas* submitted
[30] Gorelenkov N. *et al* 2002 *Proc. 19th Int. Conf. on Fusion Energy 2002 (Lyon, 2002)* (Vienna: IAEA) CD-ROM file TH/7-1Ra and http://www.iaea.org/programmes/ripc/physics/fec2002html/fec2002.htm
[31] The ITER Team 1999 *Nucl. Fusion* **39** 2175
[32] Kaye S.M. *et al* 1997 *Nucl. Fusion* **37** 1303
[33] Carolan P.G. *et al* 2002 *Proc. 19th Int. Conf. on Fusion Energy 2002 (Lyon, 2002)* (Vienna: IAEA) CD-ROM file EX/C2-6 and http://www.iaea.org/programmes/ripc/physics/fec2002html/fec2002.htm
[34] Maingi R. *et al* 2002 *Proc. 19th Int. Conf. on Fusion Energy 2002 (Lyon, 2002)* (Vienna: IAEA) CD-ROM file EX/C2-5 and http://www.iaea.org/programmes/ripc/physics/fec2002html/fec2002.htm
[35] Sykes A. *et al* 2001 *Phys. Plasmas* **8** 2101
[36] Sykes A. *et al* 2000 *Phys. Rev. Lett.* **84** 495
[37] Kotschenreuther M. *et al* 1995 *Comput. Phys. Commun.* **88** 128
[38] LeBlanc B. *et al* 2002 Confinement studies of auxiliary heated NSTX plasmas *Proc. 19th Int. Conf. (Lyon, 2002)* EX/C5-2
[39] Zweben S. *et al* 2002 *Phys. Plasmas* **9** 1981
[40] Synakowski E.J. *et al* 2002 *Plasma Phys. Control. Fusion* **44** A165
[41] Brambilla M. 1999 *Plasma Phys. Control. Fusion* **41** 1
[42] Mau T.K. *et al* 1999 *Proc. 13th Top. Conf. on Applications of RF Power to Plasmas (Annapolis, MD)* (Melville: American Institute of Physics) p 148
[43] Laqua H.P. *et al* 1998 *Phys. Rev. Lett.* **81** 2060
[44] Shevchenko V. *et al* 2001 *Proc. 28th EPS Conf. on Controlled Fusion and Plasma Phys. (18–22 June 2001)* vol 28A (ECA) p 1285
[45] Jones B. *et al* 2003 *Phys. Rev. Lett.* **90** 165001
[46] Raman R. *et al* 2001 *Nucl. Fusion* **41** 1081
[47] Raman R. *et al* 2003 *Phys. Rev. Lett.* **90** 75075